Electronic Supplementary Material (ESI) for Inorganic Chemistry Frontiers.

Enhanced photocatalytic CO_2 reduction by controlled oxygen vacancy generation and co-constructed heterojunction strategy for Pd/CeO_2

Fanlin Kong, Xiaoyan Lu, Jing Xie*, Zhenjiang Lu, Jindou Hu, Yali Cao*

State Key Laboratory of Chemistry and Utilization of Carbon Based Energy Resources, College of Chemistry, Xinjiang University, Urumqi, Xinjiang 830017, P. R. China

*Corresponding author.

Emails: caoyali523@163.com (Y.L. Cao); xiejing@xju.edu.cn (J. Xie).

Experimental

Materials

All chemicals are used as received without further purification. Cerium (III) nitrate hexahydrate ($Ce(NO_3)_3 \cdot 6H_2O$), and sodium hydroxide (NaOH) were purchased from Aladdin Reagent. Palladium nitrate dihydrate Pd ⩾ 39% ($Pd(NO_3)_2 \cdot 2H_2O$), nitric acid (HNO_3), diethylene glycol, and acetone were purchased from Sinopharm Chemical Reagent Co. Ltd. (China).

Synthesis of the CeO_2

Generally, 0.1085 g (2.5 mmol) of $Ce(NO_3)_2\ 6H_2O$ was weighed and mixed with 5 mL of diethylene glycol using ultrasound. 2 mL of HNO_3 was added dropwise and the mixture was stirred for 10 min. Then, 35 mL of acetone was poured in and the stirring continued for 20 min. After stirring, the mixture was transferred into a 100 mL Teflon-liner placed in a stainless-steel autoclave, and kept in an electric oven at 100°C for 10 h. It was then allowed to cool naturally. The resulting precursor was washed multiple times with deionized water and ethanol, and dried under natural conditions. Finally, the sample was annealed at 550°C for 4 h in the air.

Synthesis of the CeO_2-Vo

CeO_2 powder was introduced into a tube furnace and 5% H_2/Ar mixed gas was passed through it. After flowing for 20 min, the temperature was gradually increased to 400°C at a heating rate of 5°C/min and maintained at 400°C for 2 h. The catalyst obtained was labeled as CeO_2-Vo

Characterization

The X-ray diffraction (XRD, Bruker D8 Advance) of the resulting product is characterized using Cu-Kα radiation (λ=1.54056 Å) with the operating voltage of 40 kV and the working current of 40 mA during 10 ~ 80° at a scanning rate of 2° min^{-1}. The morphology

observation is performed by the field emission scanning electron microscope (FESEM, Hitachi S-4800H) with an accelerating voltage of 5 kV, transmission electron microscopy (TEM, Hitachi H-600) with an accelerating voltage of 120 kV, and high resolution transmission electron microscope (HRTEM, JEOL JEM-2010F) with an accelerating voltage of 200 kV. The element composition of samples is analyzed by energy-dispersive X-ray spectroscopy (EDS, EDAXTLS) with an operating voltage of 30 kV. Raman spectra of all samples are recorded to determine the structural properties of samples at the condition of ambient temperature on a HORIBA, France. Raman spectrum is recorded on a Raman spectrometer (HR Evlution, λ=325 nm). The surface components of the electrocatalysts are analyzed by employing an X-ray photoelectron spectrometer (XPS, Thermo Fisher Scientific ESCALAB250Xi). *In situ* FTIR measurements are conducted using the Bruker INVENIO R FT-IR spectrometer equipped with an in situ diffuse reflectance cell (Harrick). *In situ* EPR measurements are conducted using BRUKE A300. Steady-state photoluminescence spectra (PL) are used to determine the fluorescence intensity of the sample and analyze the complex separation efficiency of photogenerated carriers (Hitachi F-4500). Time-resolved photoluminescence spectra analytical characterization using the FLS-1000 instrument. The appropriate excitation wavelength is set according to the sample UV-vis diffuse reflectance data with a slit of 5 nm, and the test range is 300-700 nm (Hitachi UV-3900H). Temperature-programmed desorption of CO_2 (CO_2-TPD) is conducted on a Thermo TPDRO 1100 series.

Photoelectrochemical (PC) and cyclic voltammetry (CV) measurements are performed by the three-electrode system on an electrochemical workstation (CHI760E). Typically, the Pt net is employed as the counter electrode, the Ag/AgCl electrode is the reference electrode, and the working electrode is ITO glass coated with photocatalysts. For the preparation of the working electrode, the catalyst (5 mg) is dispersed in methanol (80 μL). After sonicating for 20 min, the mixture is deposited on the surface of the electroconductive glass (the area is 1

cm^2) and dried to form one thin film at 80°C. The Na_2SO_4 solution (0.5 $mol \cdot L^{-1}$) acted as an electrolyte. The test environment of transient photocurrent in this system is to switch the lights on and off every 30s, and the catalysts are excited by the Xe lamp (300 W). Mott-Schottky experiments were performed with 500-2000 Hz frequencies, and the test frequency of electrochemical impedance spectra (EIS) ranged from 0.1 to 100,000 Hz.

Photocatalytic activity is tested using the Labsolar-6A system containing a sealed glass photocatalytic reactor. First, 1 mL of triethanolamine is dissolved in 5 mL of deionized water, and 2 mg of photocatalyst is added and dispersed ultrasonically, then added 20 mL of acetonitrile. The solution is transferred to a 50 mL airtight quartz photocatalytic reactor. After the reactor is evacuated, it is detected using gas chromatography. Without O_2 and N_2 in the reactor, the reactor solution is purged with high purity gas of CO_2 slowly and uniformly for 30 min and the pressure is maintained at approximately 80 kPa. For the catalytic process, a 300 W Xe lamp (PLS-SXE300D) acted as the light source. The temperature of the reactor is maintained at room temperature by thermostatic water circulation. Every hour, gaseous products are analyzed using an online gas chromatography system equipped with a thermal conductivity detector (TCD) and a flame ionization detector (FID). Specifically, carbon-containing products are measured using the FID. Argon is used as the carrier gas, and the whole process took 6 h. Peak positions and areas are analyzed to determine the category and yield of products on photocatalytic CO_2 conversion. The selectivity is calculated according to the following formula:

$$\text{CO Selectivity (\%)} = 2n(\text{CO}) / [2n(\text{CO}) + 8n(\text{CH}_4)] \times 100\%$$

where $n(\text{CO})$ and $n(\text{CH}_4)$ represent the yield of CO and CH_4 during our experiment.

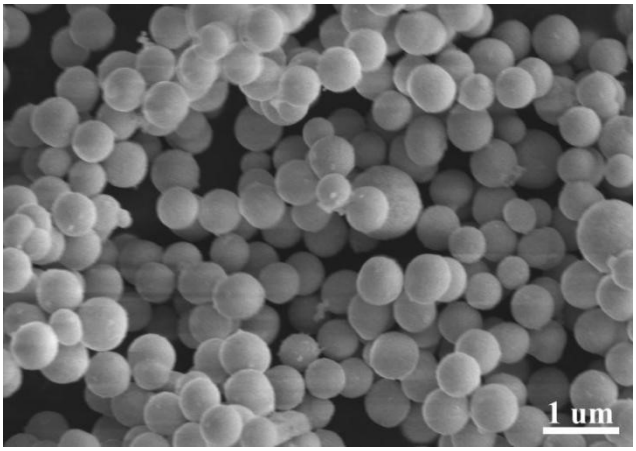

Fig. S1 The FESEM images of CeO_2.

Table S1 Surface compositions and oxidation states of catalysts derived from XPS analysis.

Catalyst	$Ce^{3+}/(Ce^{3+} + Ce^{4+})$ (%)	Vo (%)
CeO_2	22.55	13.48
CeO_2-Vo	22.67	17.49
Pd/CeO_2-Vo(p)	23.48	24.79
Pd/CeO_2-Vo(r)	24.24	26.78
Pd/CeO_2-Vo(re)	24.38	27.96
Pd/CeO_2-300	18.07	17.51
Pd/CeO_2-400	19.65	18.62
Pd/CeO_2-500	20.06	20.32

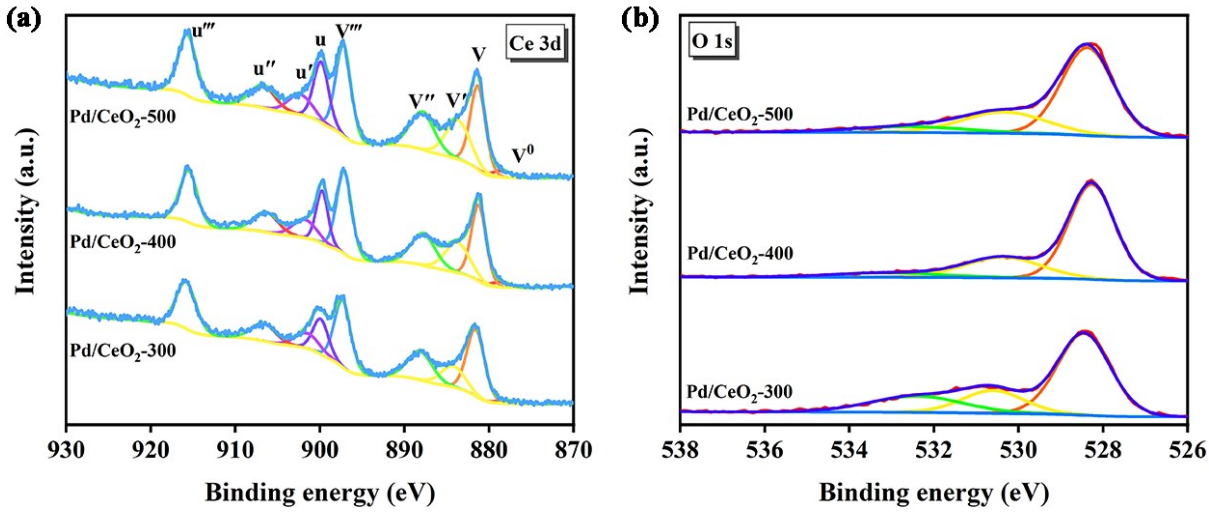

Fig. S2 High-resolution XPS spectra of (a) Ce 3d and (b) O 1s.

To investigate the effect of a reducing atmosphere on oxygen vacancy concentration, we calcined CeO_2 with the same Pd loading at 300°C, 400°C and 500°C in high-purity Ar, denoted as Pd/CeO_2-300, Pd/CeO_2-400, and Pd/CeO_2-500, respectively.

Table S2 Pd actual contents of catalysts.

Catalyst	Pd content (wt%) [a]
Pd/CeO_2-Vo(p)	0.532
Pd/CeO_2-Vo(r)	0.521
Pd/CeO_2-Vo(re)	0.524

[a] Determined by ICP-OES.

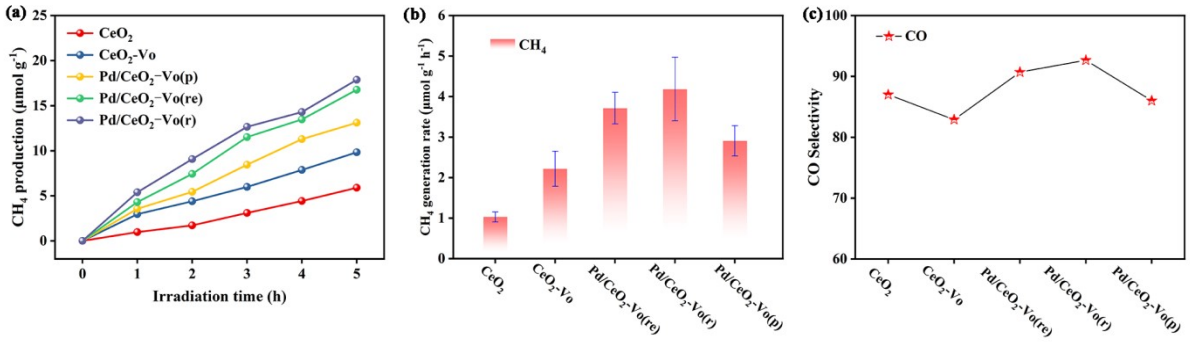

Fig. S3 (a) Production of CH_4 as functions of reaction time over samples, (b) Production rates of photocatalytic CO_2 reduction after irradiation for 5 h, (c) CO selectivity values of different samples.

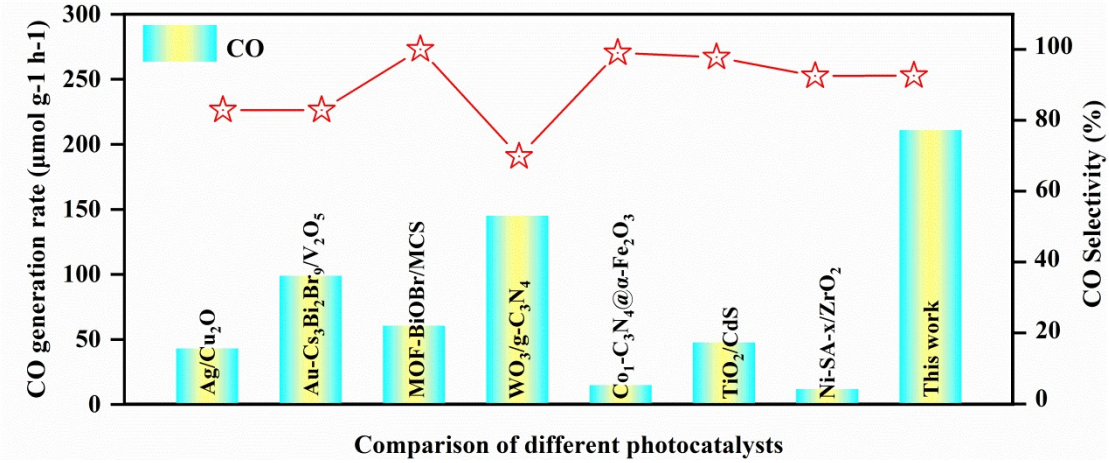

Fig. S4 Comparison of CO_2RR performance of Pd/CeO_2-Vo(r) with other reported photocatalysts.

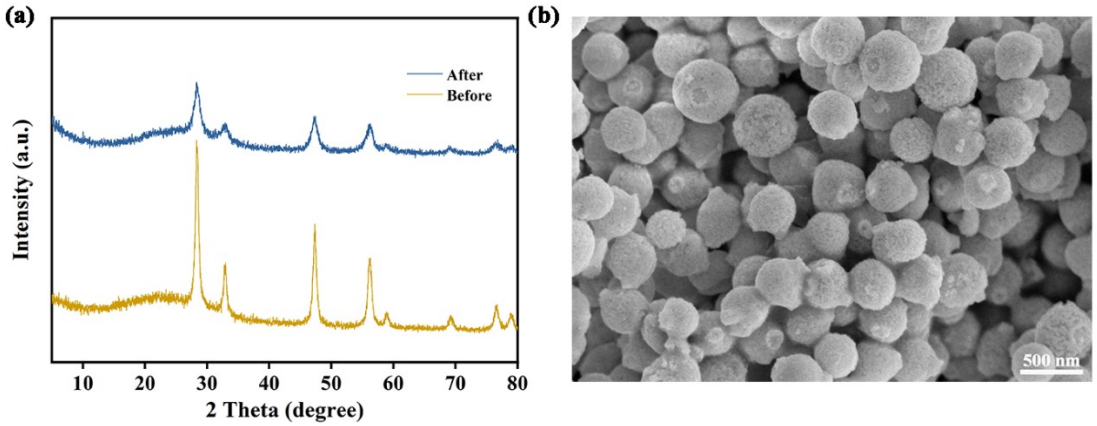

Fig. S5 (a) XRD spectra comparison before and after reaction of Pd/CeO_2-Vo(r), (b) SEM of Pd/CeO_2-Vo(r) after reaction.

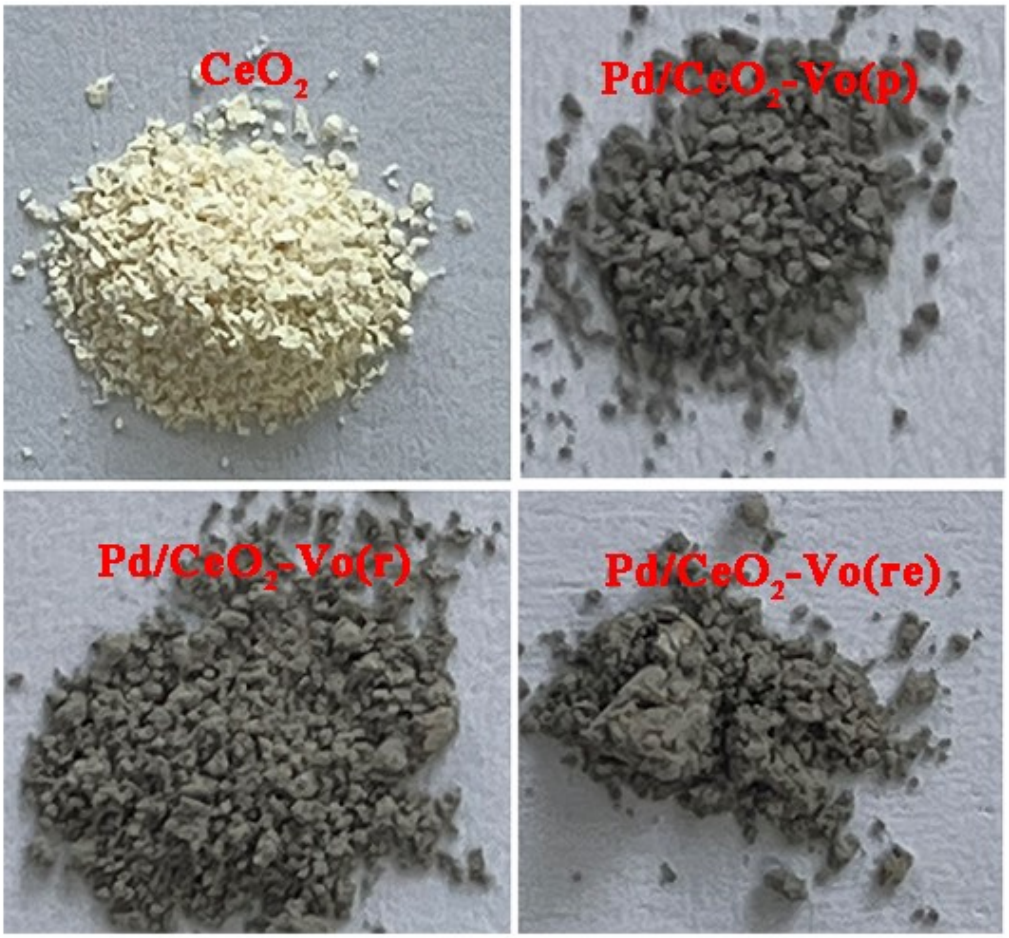

Fig. S6 Digital photos of different samples.

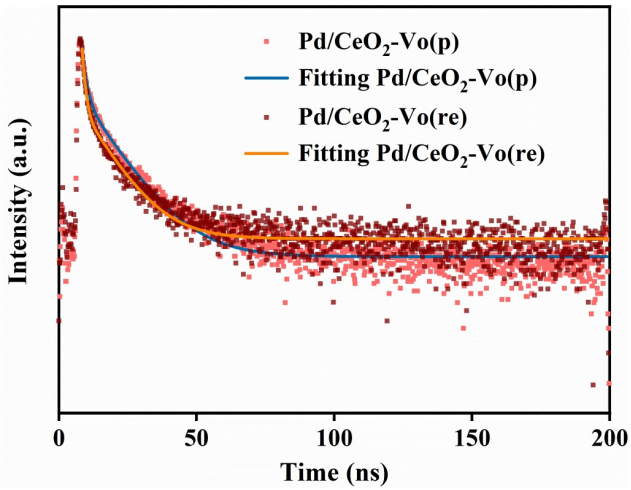

Fig. S7 Time-resolved fluorescence emission decay spectra of Pd/CeO_2-Vo(p) and Pd/CeO_2-Vo(re).

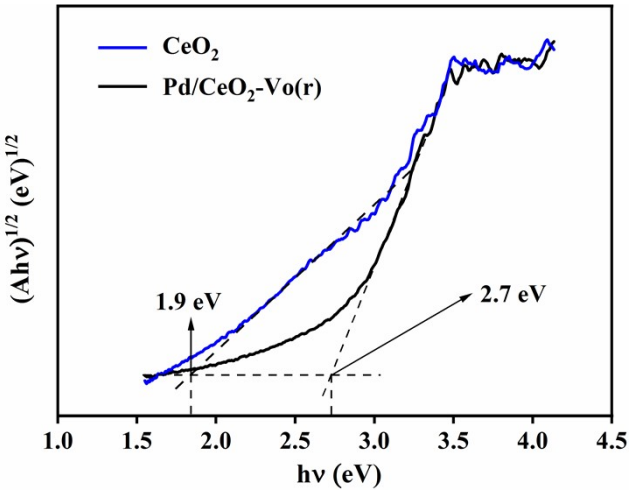

Fig. S8 Eg estimated by plotting $(\alpha h\nu)^{1/2}$ versus hν.

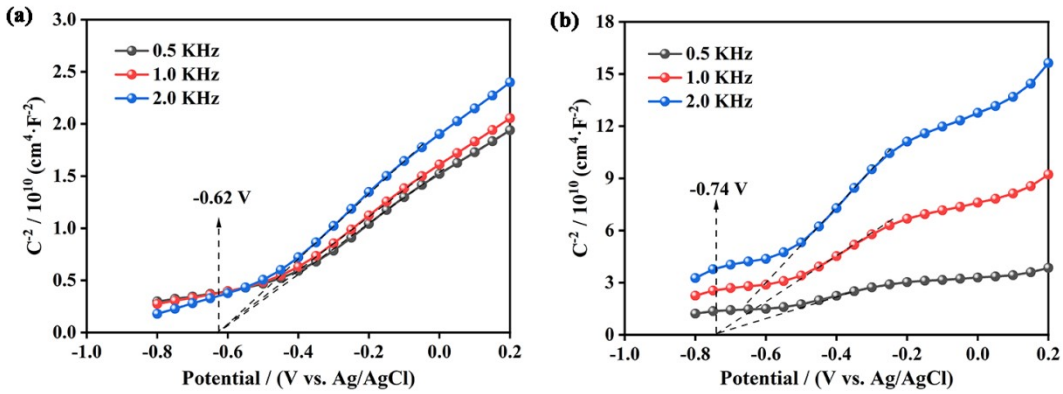

Fig. S9 Mott-Schottky plots of (a) Pd/CeO_2-Vo(p) and (b) Pd/CeO_2-Vo(re).

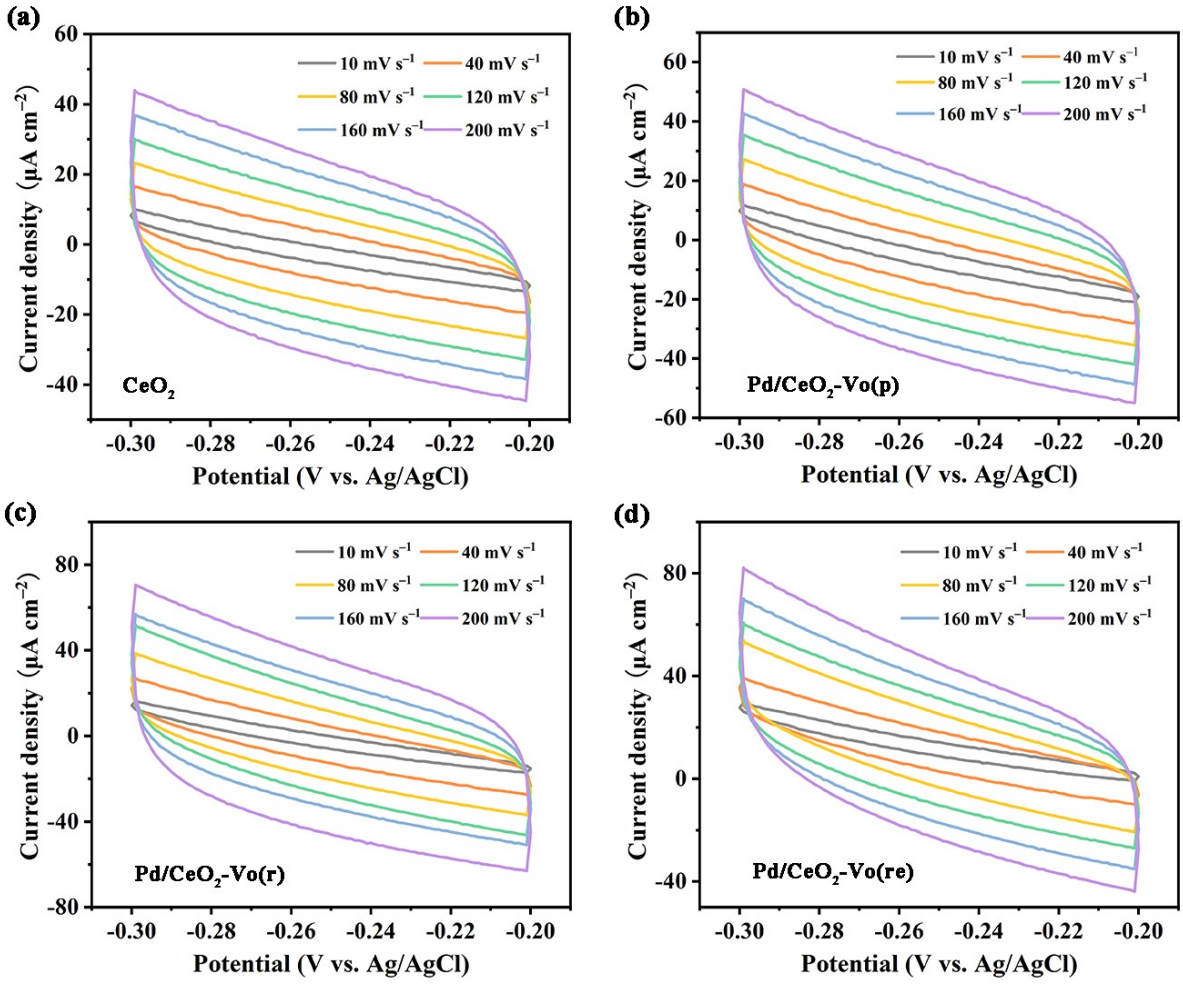

Fig. S10 CV curves of (a) CeO_2, (b) Pd/CeO_2-Vo(p), (c) Pd/CeO_2-Vo(r) and (d) Pd/CeO_2-Vo(re).

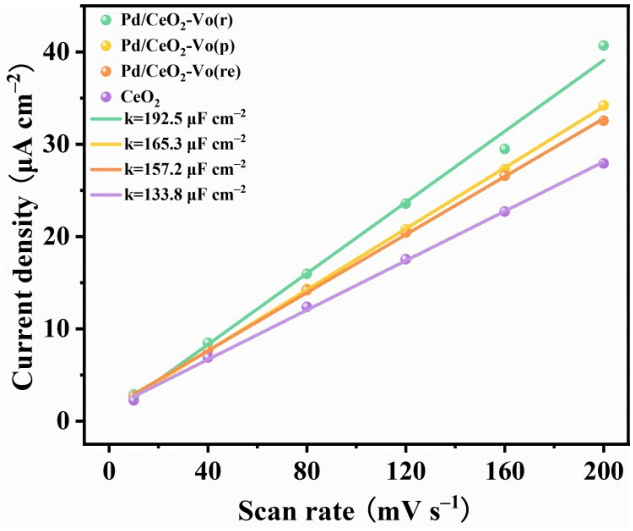

Fig. S11 The fitting curve between the capacitance and scanning rate.

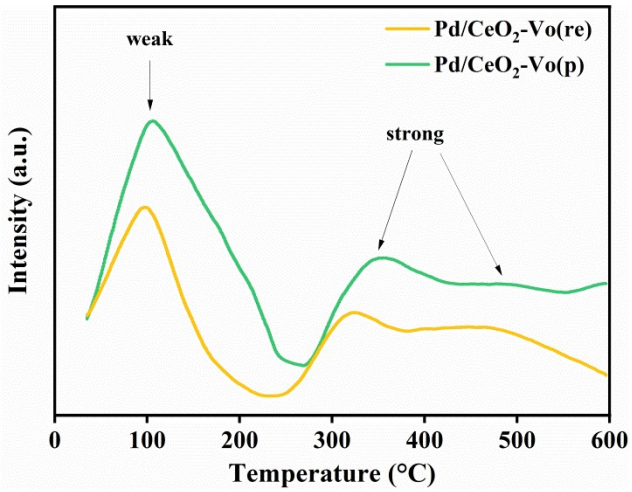

Fig. S12 CO_2-TPD curves for Pd/CeO_2-Vo(re) and Pd/CeO_2-Vo(p).

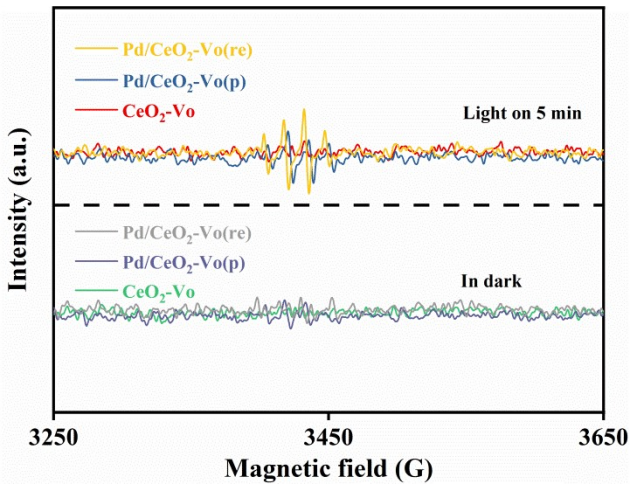

Fig. S13 ESR spectra of •OH radical (trapped by DMPO in water).

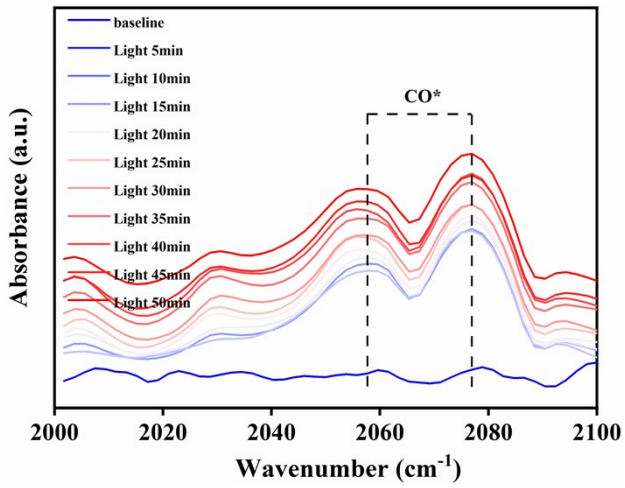

Fig. S14 *In situ* FTIR spectra of Pd/CeO_2-Vo(r) from 2000 to 2100 cm^{-1}.

Table S3 Data comparison of photocatalytic CO_2 reduction over different catalysts.

Photocatalysts	Light sources	Sacrificial agent	CH_4 selectivity	Photocatalytic efficiencies	Ref.
Vo-R-Pd/CeO_2	300 W Xe lamp	TEOA	94.10%	77.9 μmol/g/h	This work
Ag/Cu_2O	300 W Xe lamp >420 nm	H_2O	82.9%	43.04 μmol/g/h	[1]
Au-$Cs_3Bi_2Br_9$/V_2O_5	300 W Xe lamp	H_2O	98.74%	98.95 μmol/g/h	[2]
MOF-BiOBr/MCS	300 W Xe lamp >420 nm	H_2O	~ 100%	60.59 μmol/g/h	[3]
WO_3/g-C_3N_4	300 W Xe lamp	H_2O	69.79%	145 μmol/g/h	[4]
Co_1-C_3N_4@α-Fe_2O_3	300 W Xe lamp >400 nm	H_2O	> 99%	14.9 μmol/g/h	[5]
TiO_2/CdS	300 W Xe lamp	$[Ru(bpy)_3]Cl_2 \cdot 6H_2O$ TEOA + acetonitrile	97.8%	47.67 μmol/g/h	[6]
Ni-SA-x/ZrO_2	300 W Xe lamp	H_2O	92.5%	11.8 μmol/g/h	[7]

References

[1] S.H. Ding, X.H. Bai, L.K. Cui, Q.Q. Shen, X.L. Zhang, H.S. Jia and J.B. Xue, Ag as an electron mediator in porous Cu_2O nanostructures for photocatalytic CO_2 reduction to CO, *ACS Appl. Nano Mater.*, 2023, **6** 10539–10550.

[2] H. Fu, X.L. Liu, Y.Q. Wu, Q.Q. Zhang, Z.Y. Wang, Z.K. Zheng, H.F. Cheng, Y.Y. Liu, Y. Dai, B.B. Huang and P. Wang, Construction of a bismuth-based perovskite direct Z-scheme heterojunction Au-$Cs_3Bi_2Br_9$/V_2O_5 for efficient photocatalytic CO_2 reduction, *Appl. Surf. Sci.*, 2023, **622**, 156964.

[3] J.H. Hua, Z.L. Wang, J.F. Zhang, K. Dai, C.F. Shao and K. Fan, A hierarchical Bi-MOF-derived BiOBr/Mn0.2Cd0.8S S-scheme for visible-light-driven photocatalytic CO_2 reduction, *J. Mater. Sci. Technol.*, 2023, **156**, 64–71.

[4] B. Tahir, M. Tahir and M.G.M. Nawawi, Highly stable 3D/2D WO_3/g-C_3N_4 Z-scheme

heterojunction for stimulating photocatalytic CO_2 reduction by H_2O/H_2 to CO and CH_4 under visible light, *J. CO_2 Util.*, 2020, **41**, 101270.

[5] B.C. He, C. Zhang, P.P. Luo, Y. Li and T.B. Lu, Integrating Z-scheme heterojunction of Co_1-C_3N_4@α-Fe_2O_3 for efficient visible-light-driven photocatalytic CO_2 reduction, *Green Chem.*, 2020, **22**, 7552–7559.

[6] Z.H. Chen, D.P. Li and C.J. Chen, Urchin-like TiO_2/CdS nanoparticles forming an S-scheme heterojunction for photocatalytic hydrogen production and CO_2 reduction, *ACS Appl. Nano Mater.*, 2023, **6**, 21897–21908.

[7] X.Y. Xiong, C.L. Mao, Z.J. Yang, Q.H. Zhang, G.I.N. Waterhouse, L. Gu and T.R. Zhang, Photocatalytic CO_2 reduction to CO over Ni single atoms supported on defect-rich zirconia, *Adv. Energy Mater.*, 2020, **10**, 2002928.